

The high-temperature and high-pressure behavior of MgO derived from lattice vibration calculations. Kieffer's model revisited

Michel H. G. Jacobs* and Bernard H. W. S. de Jong

Geodynamics Research Institute, Utrecht University, Budapestlaan 4, NL-3584, CD Utrecht, The Netherlands

Received 7th February 2003, Accepted 1st April 2003

First published as an Advance Article on the web 17th April 2003

The model of Kieffer has been extended and applied to derive thermodynamic properties from the lattice vibrational behavior of pure substances. The model for MgO has been validated in the pressure range between 0 and 300 GPa and temperature range between 100 and 4000 K. The model is constrained by thermodynamic data, lattice vibrational frequencies and data on transverse and longitudinal sound velocities. It is shown that intrinsic anharmonicity is present in the different modes of vibration. It is concluded that the accuracy of the results is not significantly affected by using different equations of state for the principal isotherm. It is shown that all thermodynamic data and sound wave velocity data are accurately described except for shock-wave data. The model of Kieffer is contrasted with the Mie–Grüneisen–Debye model and it is shown that the former represents more accurately experimental thermodynamic and longitudinal and transverse sound wave velocity data.

1 Introduction

Thermodynamic functions are important tools to predict chemical equilibria between substances at conditions inaccessible to experimentation or in those regions of pressure and temperature where experiments are not available. These tools can be used to construct a thermodynamic database for materials of geophysical relevance. Emphasis is placed on the critical assessment of the complete set of experimental data of all phases in the quinary system MgO–FeO–SiO₂–Al₂O₃–CaO. A series of internally consistent databases have been developed for the quinary system or parts of it, *e.g.* Fei *et al.*,¹ Saxena,² Gottschalk,³ Chatterjee *et al.*,⁴ Fabrichnaya⁵ and Holland and Powell.⁶ However, these databases cannot be used to derive longitudinal, transverse sound wave velocities and the shear modulus of materials at earth mantle conditions, properties of particular interest in the field of seismology and mantle rheology. To extend the application of our database to the field of seismology, we have programmed and validated a quantum-thermodynamical method based on lattice vibrations with the aim to calculate and predict thermodynamic properties, longitudinal and transverse sound velocities at any pressure and temperature. The method finds its origin in the pioneering work of Kieffer,^{7,8} who introduced an elegant method to calculate thermodynamic properties from lattice vibrations as a function of temperature for silicate minerals at 1 bar pressure. It has been noted by Kieffer^{7,8} that although the model lacks the rigor of a complete lattice dynamics theory, its successful application is rooted in the fact that thermodynamic properties are insensitive to details of the vibrational density of states. We test this statement by comparing the results of our calculations based on Kieffer's model with a Mie–Grüneisen–Debye model (see *e.g.* Jackson and Rigden⁹) for which the vibrational density of state takes a much simpler form. We used statistical thermodynamic theory to extend Kieffer's method to compute thermodynamic properties from the vibrational density of states, at arbitrary pressure and temperature. The choice of MgO is more or less obvious. It is one of the key materials for geodynamic research; it is monomorphous; in particular there are experimental thermodynamic data in the temperature

range between 100 and 4000 K and pressure range between 0 and 225 GPa. Additionally, data exist for transverse and longitudinal sound velocities in the temperature range between 300 K and 2000 K and pressure range between 0 and 60 GPa to validate our results.

2 Thermodynamic background

In an earlier paper, by Jacobs and Oonk,¹⁰ it was shown that the Gibbs energy plays a key role in the understanding of the phase behavior of matter as a function of thermodynamic temperature (T), pressure (P) and composition. In this section we relate the Gibbs energy to microscopic vibrational motions in the atomic arrays, which constitute the crystal lattice of a substance with the aim to calculate and predict thermodynamic properties, transverse and longitudinal sound velocities. The connection between macroscopic thermodynamic bulk properties and microscopic motions in a solid substance is usually accomplished by the Helmholtz energy, A . For an insulator material it can be written as:

$$A(T, V) = A(0, V) + A^{\text{vib}}(T, V), \quad (1)$$

where V represents volume. The first term on the right hand side of eqn. (1) is often referred to as the Helmholtz energy of the static lattice and represents its volume variation at $T = 0$ K. This term is computed by applying a proper equation of state. The last term represents the Helmholtz energy due to lattice vibrational motions. In experimental practice, volume measurements as a function of pressure, needed in the first term, are usually not performed at 0 K but at ambient temperature T_0 . By selecting $(T_0, P^0) = (298.15 \text{ K}, 1 \text{ bar})$ as the reference condition, eqn. (1) can be rewritten as:

$$A(T, V) = A^{\circ}(T_0) + A^{\text{eos}}(T_0, V) + A^{\text{vib}}(T, V) - A^{\text{vib}}(T_0, V), \quad (2)$$

where the superscript $^{\circ}$ in the first term on the right hand side denotes a constant pressure condition of 1 bar. The second term on the right hand side of eqn. (2) represents a term purely

dependent on volume at the reference temperature T_0 and is calculated by the introduction of an equation of state (eos). The constant $A^0(T_0)$ can be expressed in the enthalpy of formation of a substance at the reference condition by deriving the expressions for the entropy and enthalpy. From eqn. (2) it follows that the entropy is written as:

$$S(T, V) = -\left(\frac{\partial A}{\partial T}\right)_V = S^{\text{vib}}(T, V), \quad (3)$$

and the enthalpy as:

$$H(T, V) = A + TS + PV = A^0(T_0) + A^{\text{eos}}(T_0, V) + U^{\text{vib}}(T, V) - A^{\text{vib}}(T_0, V) + PV \quad (4)$$

The term $A^{\text{eos}}(T_0, V)$ is defined as:

$$A^{\text{eos}}(T_0, V) = -\int_{V^0(T_0)}^V P^{\text{eos}}(T_0, V) dV, \quad (5)$$

where $P^{\text{eos}}(T_0, V)$ represents the equation of state expression at the reference isotherm defined by T_0 , and $V^0(T_0)$ the volume at the reference condition. From eqn. (5) it follows that $A^{\text{eos}}(T_0, V)$ vanishes at the reference condition (T_0, P^0) and the constant $A^0(T_0)$ is therefore expressed as:

$$A^0(T_0) = \Delta H_f^0 - U^{\text{vib}}(T_0, V^0(T_0)) + A^{\text{vib}}(T_0, V^0(T_0)) - P^0 V^0(T_0), \quad (6)$$

where $\Delta H_f^0 = H(T_0, V^0(T_0))$ represents the enthalpy of formation at the reference condition.

To complete the thermodynamic background, we write the expression for the pressure derived from eqn. (2) as:

$$P(T, V) = -\left(\frac{\partial A}{\partial V}\right)_T = P^{\text{eos}}(T_0, V) + P^{\text{vib}}(T, V) - P^{\text{vib}}(T_0, V) \quad (7)$$

where P^{vib} represents the so-called thermal part of pressure. Here we arrive at one of the key points of the underlying paper, which is, that we have a means to discriminate between different equations of state for the representation of experimental data. We shall investigate the difference in representation of experimental data by using (i) a third order Birch–Murnaghan equation of state and (ii) the equation of state of Jacobs and Oonk.¹⁰

In thermodynamic practice the determination of the Gibbs energy differs from what we have presented in a previous paper from our department, Jacobs and Oonk.¹⁰ It is generally carried out as follows. Provided that an equation of state has been selected and that expressions for the vibrational parts of the Helmholtz energy and entropy are available, the volume at the experimental condition (T, P) is numerically evaluated using eqn. (7). In the next step the calculated volume is used to determine the Helmholtz energy given by eqn. (2), which leads to the Gibbs energy by applying the relation $G = A + PV$.

3 Quantum mechanical background

The simplest approach to determine the vibrational part of thermodynamic functions of a crystal is accomplished within the framework of a harmonic approximation in which Hooke's law is obeyed. In this case, the solution of the Schrödinger equation for an individual oscillator leads to a simple expression for the eigenvalues, ε_n , describing the energy states. The vibrational partition function, Z^{vib} , is given by statistical mechanics as:

$$Z^{\text{vib}} = \sum_{n=0}^{\infty} \exp\left(\frac{-\varepsilon_n}{kT}\right) = \sum_{n=0}^{\infty} \exp\left(-\left(n + \frac{1}{2}\right) \frac{\hbar\omega}{kT}\right) = \frac{\exp\left(-\frac{\hbar\omega}{2kT}\right)}{1 - \exp\left(-\frac{\hbar\omega}{kT}\right)}, \quad (8)$$

where k denotes Boltzmann's constant, \hbar is Planck's constant divided by 2π and ω the angular frequency of the oscillator. Thermodynamic properties are readily derived from the partition function by recognizing that ω is a function of T and V ; e.g. the Helmholtz energy for a single (Einstein) oscillator is given by:

$$A_{\text{single}}^{\text{vib}} = -kT \ln(Z^{\text{vib}}) = kT \left(\frac{\hbar\omega}{2kT} + \ln\left(1 - \exp\left(-\frac{\hbar\omega}{kT}\right)\right) \right), \quad (9)$$

The thermodynamic functions of the crystal are expressed as averages over the vibrational density of states $g(\omega)$. The product $g(\omega)d\omega$ represents the fraction of oscillators in the frequency interval between ω and $\omega + d\omega$. For instance, the vibrational part of the Helmholtz energy in eqn. (2) becomes:

$$A^{\text{vib}}(T, V) = \int_0^{\omega_{\text{max}}} A_{\text{single}}^{\text{vib}}(\omega) g(\omega) d\omega, \quad (10)$$

where ω_{max} represents the highest measured angular frequency.

For a Debye model $g(\omega)$ is written as:

$$g(\omega) = \frac{9nN_A\omega^2}{\omega_{\text{max}}^3} \delta, \quad (11)$$

where N_A is Avogadro's number, n the number of atoms per molecule ($n = 2$ for MgO), ω_{max} is the Debye cut-off angular frequency and δ Kronecker's delta ($\delta = 1$ for $\omega \leq \omega_{\text{max}}$ and $\delta = 0$ for $\omega > \omega_{\text{max}}$). The cut-off frequency is related to the well-known Debye temperature by $\theta_D = \hbar\omega/k$. In the Debye model it is assumed that all acoustic waves travel with the same velocity and hence that the solid is elastically isotropic. Kieffer's model takes into account the more realistic situation that most solids are elastically anisotropic. In her model, three acoustic modes of vibrations are defined, one longitudinal mode and two transverse modes. Each of the three acoustic modes is characterized at long wavelengths by a directionally averaged sound velocity. For Kieffer's model $g(\omega)$ is written as:

$$g(\omega) = \frac{3N_A}{Z} \left(\frac{2}{\pi}\right)^3 \sum_{i=1}^3 \left(\frac{\arcsin^2(\omega/\omega_i)}{(\omega_i^2 - \omega^2)^{1/2}} \delta_i \right) + \left(3n - \frac{3}{Z}\right) N_A \sum_{j=1}^{N_{\text{oc}}} \left(\frac{f_j}{\omega_{u_j} - \omega_l} \delta_j \right), \quad (12)$$

with the conditions: $\delta_i = 1$ for $\omega \leq \omega_i$ and $\delta_i = 0$ for $\omega > \omega_i$, and $\delta_j = 1$ for $\omega_l \leq \omega \leq \omega_{u_j}$ and $\delta_j = 0$ for $\omega(\omega_l$ or $\omega) \omega_{u_j}$.

In eqn. (12), Z is the number of molecules in the primitive cell ($Z = 1$ for MgO). The first term on the right hand side describes the contributions due to acoustic lattice vibrations having constant group velocities. These lattice waves are dispersive in nature because the phase velocity depends on the frequency of the lattice vibration. In the model a simple sinusoidal dispersion relation has been assumed which results in the 'arcsin' function in the first term. The second term on the right hand side describes the vibrations, which are not in phase. Because MgO consists of atoms having opposite charges, these vibrations may interact with the electric field of electromagnetic radiation. This type of vibration is therefore called optic mode of vibration. We have extended Kieffer's original theory by recognizing the presence of multiple optic

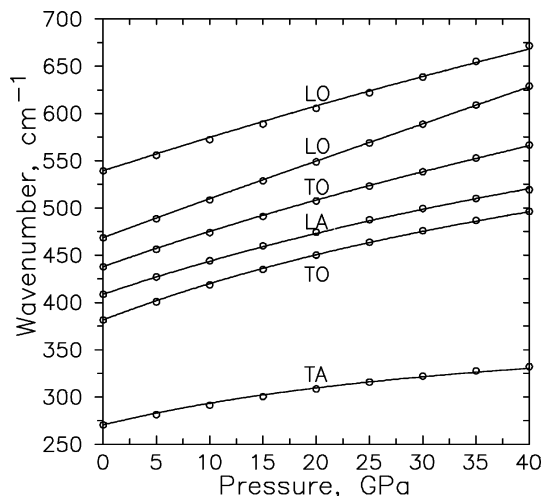


Fig. 1 Calculated wavenumbers ($\omega/(2\pi c)$, with c the speed of light) of six vibrational modes in MgO compared with the experimental data from Chopelas.¹² The experimental error is claimed to be smaller than the symbol size. LO denotes a longitudinal optic mode, LA a longitudinal acoustic mode, TO a transverse optic mode and TA a transverse optic mode.

modes of vibration in a crystal, N_{OC} being the number of optic modes and f_j the fraction of the total number of optic oscillators in mode j . This enables us to constrain the thermodynamic description for MgO with experimental data on pressure variation of the vibrational frequency of each mode as shown in Fig. 1. The change of the vibrational frequency of a mode j with pressure is indirectly described by the classical expression derived by Grüneisen:¹¹

$$\gamma_j = -\left(\frac{\partial \ln \omega_j}{\partial \ln V}\right)_T = +\frac{K}{V}\left(\frac{\partial \omega_j}{\partial P}\right)_T, \quad (13)$$

where γ_j represents the so-called Grüneisen parameter and K the isothermal bulk modulus. Fig. 1 and eqn. (13) show that a positive Grüneisen parameter results in an increase of the vibrational frequencies when pressure is increased. The experiments show that MgO must at least be described within the quasi-harmonic approximation in which the frequencies depend on volume. In the approximation it is assumed that the frequencies do not change with temperature at constant volume. This is in contrast with the harmonic approximation in which the frequencies do not depend on pressure and temperature. In our description of experimental thermodynamic data and sound velocities, it appeared that the vibrational frequencies change with temperature at constant volume. In analogy with Gillet *et al.*,¹³ this is called an effect of intrinsic anharmonicity. We have adopted a method given by these authors to obtain an expression for the vibrational frequency of a mode j , which include all the mentioned effects. This is accomplished by expanding the logarithm of angular frequency of a vibrational mode in a Taylor series of $\ln(V)$ and T . Dropping the subscript j and expanding to the third power in $\ln(V)$ and T , we write:

$$\begin{aligned} \ln\left(\frac{\omega}{\omega^0}\right) = & -\gamma^0 \ln\left(\frac{V}{V^0}\right) + a^0(T - T_0) - \frac{1}{2}q_0^0 \gamma^0 \ln^2 \\ & \times \left(\frac{V}{V^0}\right) - \frac{1}{6}q_0^0 \gamma^0 (q_0^0 + q_1^0) \ln^3\left(\frac{V}{V^0}\right) \\ & + m^0(T - T_0) \ln\left(\frac{V}{V^0}\right) + \frac{1}{2}(-\gamma^0 k_1^0 + q_0^0 m^0) \\ & \times (T - T_0) \ln^2\left(\frac{V}{V^0}\right) + \frac{1}{2}m_1^0 (T - T_0)^2 \\ & + \frac{1}{2}k_2^0 (T - T_0)^2 \ln\left(\frac{V}{V^0}\right) + \frac{1}{6}k_3^0 (T - T_0)^3 \end{aligned} \quad (14a)$$

where the superscript 0 denotes the reference condition. The constants in expression (14a) are given by:

$$\begin{aligned} \gamma^0 = & -\left(\frac{\partial \ln \omega}{\partial \ln V}\right)_R, \quad a^0 = \left(\frac{\partial \ln \omega}{\partial T}\right)_R, \quad q_0^0 = \left(\frac{\partial \ln \gamma}{\partial \ln V}\right)_R, \\ q_1^0 = & \left(\frac{\partial \ln q}{\partial \ln V}\right)_R, \quad m^0 = \left(\frac{\partial^2 \ln \omega}{\partial \ln V \partial T}\right)_R = -\left(\frac{\partial \gamma}{\partial T}\right)_R, \\ m_1^0 = & \left(\frac{\partial^2 \ln \omega}{\partial T^2}\right)_R = \left(\frac{\partial a}{\partial T}\right)_R, \quad k_1^0 = \left(\frac{\partial q}{\partial T}\right)_R, \\ k_2^0 = & \left(\frac{\partial^3 \ln \omega}{\partial \ln V \partial T^2}\right)_R = -\left(\frac{\partial^2 \gamma}{\partial T^2}\right)_R, \\ k_3^0 = & \left(\frac{\partial^3 \ln \omega}{\partial T^3}\right)_R = \left(\frac{\partial^2 a}{\partial T^2}\right)_R, \end{aligned} \quad (14b)$$

where subscript R denotes the reference condition. The constants in eqn. (14) can be determined experimentally by measuring the vibrational frequencies as a function of pressure and temperature. In the underlying work we have determined the constants by means of a least squares fit of all available experimental data.

Finally, Kieffer's theory relates the directionally averaged sound velocities, u_i , of the transverse and longitudinal waves to their cut-off angular vibrational frequencies $\omega_{i, \max}$ as:

$$u_i = \frac{1}{4} \left(\frac{4\pi ZV}{3N_A} \right)^{1/3} \omega_{i, \max}, \quad (15)$$

where the subscript $i = 1, 2$ or 3 has the same meaning as in eqn. (12). In the following we denote u_1 and u_2 as the sound velocities of the transverse waves and u_3 as that of the longitudinal wave. As has been stated by Kieffer,⁷ a problem arises to determine two characteristic transverse sound velocities because the only data available are single Voigt–Reuss–Hill averaged transverse sound velocities (v_T). One of her assumptions to solve this problem is that the following relation is applicable:

$$\frac{2}{v_T^3} = \frac{1}{u_1^3} + \frac{1}{u_2^3}. \quad (16)$$

This means that in our computations, we can determine v_T as a function of pressure and temperature by calculating the frequencies $\omega_1(P, T)$ and $\omega_2(P, T)$ by the application of eqn. (14) and $u_1(P, T)$ and $u_2(P, T)$ by the application of eqn. (15). In our computations we have adopted the values for u_1 , u_2 and u_3 given by Kieffer⁸ leading to the cut-off frequencies $\omega_{i, \max}^0(T_0, \rho)$, expressed in cm^{-1} , given in Table 1. On the other hand, the formalism presented in this and the preceding section makes it possible to calculate the bulk sound velocity, v_B , from the adiabatic bulk modulus, K_S , and density, ρ , by the relation $v_B = (K_S/\rho)^{1/2}$. By applying eqns. (14) and (15) to derive the longitudinal sound velocity (v_L), the transverse sound velocity is calculated by the well-known relation in classical mechanics as:

$$v_B^2 = v_L^2 - \frac{4}{3}v_T^2 \quad (17)$$

Table 1 Properties defining the vibrational density of states used in the Kieffer model

Type of vibration	Mode	Wavenumber range/ cm^{-1}	Fraction
Acoustic, transverse	1	0.00–289.00	1.0000
Acoustic, transverse	2	0.00–312.00	1.0000
Acoustic, longitudinal	3	0.00–482.00	1.0000
Optic	4	312.00–395.05	0.18096
Optic	5	395.05–453.15	0.21358
Optic	6	453.15–482.00	0.18779
Optic	7	482.00–730.00	0.41767

In Section 5 we shall discuss the consistency of relations (16) and (17).

4 Results

We started our analysis of thermodynamic data by assuming that the vibrational spectrum can be described within the framework of a Mie–Grüneisen–Debye model.⁹ The underlying reason for this exercise was to explore the sensitivity of thermodynamic properties to details of the vibrational density of states (VDOS). The VDOS, represented by eqn. (11), takes the simple parabolic shape as depicted in Fig. 2. In a first approach we assumed that the Debye cut-off frequency depends only on volume. Its temperature dependence is therefore indirectly incorporated because the volume depends on temperature. The resulting coefficients of eqn. (14) are given in Table 2 and the calculated thermal expansivity at 1 bar pressure is depicted in Fig. 3. The calculations do not represent the measurements of Dubrovinsky and Saxena²⁰ and those of Fiquet *et al.*²² within their stated accuracy of 2% in the temperature range between 300 and 1800 K. The misfit of all thermodynamic experimental data at 1 bar pressure can be visualized by plotting the macroscopic Grüneisen parameter using the well-known relation $\gamma = \alpha K_S V / C_P$, where α denotes thermal expansivity and C_P the heat capacity at constant pressure. From Fig. 4, it is seen that the calculations do not represent the nearly temperature independent behavior of the Grüneisen parameter at temperatures above the Debye temperature. Because expanding eqn. (14) to incorporate more terms to describe the volume dependence of the cut-off frequency did not improve the accuracy of the result significantly, we concluded that this first approach does not suffice to represent experimental data at 1 bar pressure.

In a second approach, we explored Kieffer's model to incorporate more details of the VDOS. The assignment of the lower and upper cut-off frequencies of the optic modes is not obvious and to a certain extent arbitrary. The problem originates from the fact that in Kieffer's model each optic mode is represented as a uniform distribution of Einstein oscillators, each oscillator having the same weight in the vibrational spectrum. The frequency ranges as determined by the measurements of Chopelas¹² guided us to estimate the cut-off frequencies. The result of this estimate is given in Table 1. Next we determined

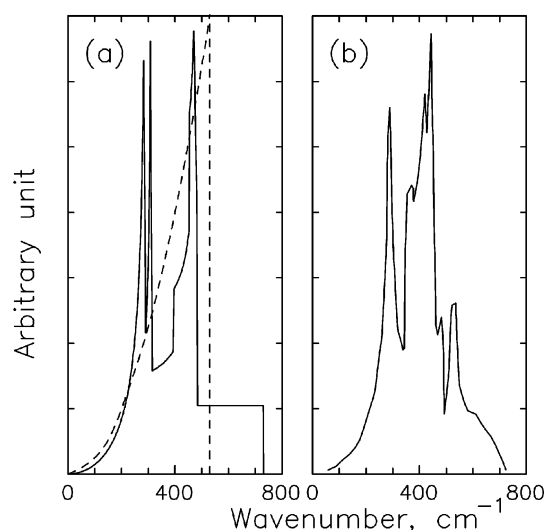


Fig. 2 Vibrational density of states (VDOS) of MgO. (a) The solid VDOS has been calculated with Kieffer's model by applying eqn. (12) and the data in Table 1. The dashed VDOS has been calculated with the MGD model by applying eqn. (11); the calculated Debye temperature, 764 K, corresponds to 530.4 cm^{-1} . (b) VDOS reported by Sangster *et al.*¹⁴ derived from inelastic neutron scattering experiments.

the fractions of the optic modes in such a way that the VDOS as derived by Sangster *et al.*¹⁴ was represented as accurately as possible. The cut-off frequencies of the acoustic and optic modes at ambient conditions together with the fractions fix the value of the entropy at ambient conditions. The calculated value for the standard entropy of about 28 $\text{J K}^{-1} \text{mol}^{-1}$ at 298.15 K is too high compared with the experimental value of $26.924 \pm 0.08 \text{ J K}^{-1} \text{mol}^{-1}$ derived from calorimetric experiments (see JANAF thermochemical Tables, Chase *et al.*²⁵). Directing the optimisation to the experimental value of the standard entropy at 298.15 K resulted in the calculated fractions given in Table 1 and a calculated VDOS presented in Fig. 2. As can be seen from Fig. 2, the calculated VDOS deviates from the experimental VDOS in the frequency range between the transverse and longitudinal modes. The reason behind this is that the cut-off frequency of the longitudinal mode is larger than the frequency of the highest experimental peak at about 450 cm^{-1} , leading to lower fractions of the optic modes in the mid-frequency range of the VDOS. We consider the deviation an artifact of Kieffer's theory because the cut-off frequency of the longitudinal mode is fixed by the experimental value of the longitudinal sound wave velocity by eqn. (15). The selection of different values for the cut-off frequencies of the optic modes indeed showed that the representation of the experimental VDOS could not be improved significantly. The result of the optimisation, in which the cut-off frequencies depend only on volume, is given in Table 2 and the resulting Grüneisen parameter is plotted in Fig. 4. Fig. 4 shows that also in Kieffer's model the nearly temperature independent behavior of the Grüneisen parameter cannot be reproduced.

In the discussion we argue that the accuracy of representing data at 1 bar pressure increases significantly by the assumption that the cut-off frequencies change with temperature at constant volume in addition to the change with volume alone.

5 Discussion

In this paper we are concerned about two different kinds of properties, thermodynamic ones and sound velocities. Both kinds of properties are described in terms of an equation of state and by vibrational motions in the crystal lattice of a substance, MgO in our particular case. In this section we discuss four items, which are important to achieve an accurate description of all properties of interest. These are (i) constraints in thermophysical properties, (ii) the volume and temperature dependence of the cut-off frequencies, (iii) the role of the equation of state, and (iv) sound wave velocities.

5.1 Constraints in thermophysical properties; anomalies

For both the MGD and the Kieffer model special care has been taken to eliminate anomalous behavior in all thermodynamic properties, in the pressure range between 1 bar and 300 GPa and the temperature range between 100 and 4000 K, ranges of particular geophysical interest. Anomalies in entropy or thermal expansivity as mentioned by Jacobs and Oonk¹⁰ do not occur. We have achieved this by putting physically realistic constraints in regularly distributed intervals in pressure and temperature space. For instance, for the face centered cubic MgO lattice with two interpenetrating cubic lattices, we have assumed the realistic constraint that compressibility increases with temperature whereas it decreases with pressure. We have constrained the Kieffer model by the additional conditions that the shear modulus (rigidity) increases with pressure and decreases with temperature and that the vibrational frequencies decrease with temperature along isobars and increase with pressure along isotherms. Because the Kieffer model contains more characteristics of the VDOS compared to the MGD formalism, it requires more parameters in terms of the

Table 2 Results of the optimisation obtained with a Kieffer and a Mie–Grüneisen–Debye model. All parameters are given at ambient conditions (298.15 K, 1 bar). K_0 represents the isothermal bulk modulus, K_0' its isothermal pressure derivative, θ_D the Debye temperature. The ambient volume is $V^0(T_0) = 11.248 \text{ cm}^3 \text{ mol}^{-1}$. All other parameters are used in eqn. (6) and (14). The abbreviation ‘eos’ denotes equation of state. A number in parenthesis denotes the uncertainty in a value

Mode	γ_0	q_0^0	q_1^0	$10^5 a^0/\text{K}^{-1}$	$10^5 m^0/\text{K}^{-1}$	$10^9 m_1^0/\text{K}^{-2}$	$10^5 k_1^0/\text{K}^{-1}$	$10^8 k_2^0/\text{K}^{-2}$
Kieffer, cut-off frequencies volume dependent, third order Birch–Murnaghan eos								
1, 2	1.58(2)	4.21(4)	-2.00(3)	0.00	0.00	0.00	0.00	0.00
3	1.64(3)	2.50(8)	0.64(5)	0.00	0.00	0.00	0.00	0.00
4	1.63(8)	0.6(3)	-6.5(6)	0.00	0.00	0.00	0.00	0.00
5	1.27(7)	-2.49(4)	8.4(1)	0.00	0.00	0.00	0.00	0.00
6	1.34(7)	-2.35(6)	-1.5(2)	0.00	0.00	0.00	0.00	0.00
7	0.97(6)	-3.05(7)	6.3(2)	0.00	0.00	0.00	0.00	0.00
$K_0 = 160.59(18) \text{ GPa}$, $K_0' = 4.04(3)$, $\theta_D = 940.38(40) \text{ K}$, $A^0(T_0) = -609.267(630) \text{ kJ mol}^{-1}$								
Kieffer, intrinsic anharmonic effect in cut-off frequencies, third order Birch–Murnaghan eos								
1, 2	1.63(2)	4.17(3)	-1.57(1)	-1.50(9)	2.1(1)	-9.7(2)	-5.0(3)	-1.61(3)
3	1.49(5)	0.816(5)	0.24(1)	-1.32(7)	0.7(1)	0.3(2)	-2.5(3)	-0.72(3)
4	1.76(6)	1.541(7)	-2.15(1)	3.4(1)	11.5(4)	0.00	0.00	0.00
5	1.55(7)	0.52(1)	-9.0(3)	1.9(1)	4.3(3)	0.00	0.00	0.00
6	1.45(5)	-2.1(2)	5.6(6)	3.0(1)	3.6(2)	0.00	0.00	0.00
7	1.04(5)	-2.8(3)	7.0(4)	0.7(1)	0.5(1)	0.00	0.00	0.00
$K_0 = 160.59(22) \text{ GPa}$, $K_0' = 4.04(2)$, $\theta_D = 940.38(40) \text{ K}$, $A^0(T_0) = -609.267(630) \text{ kJ mol}^{-1}$								
Kieffer, intrinsic anharmonic effect in cut-off frequencies, eos of Jacobs and Oonk ¹⁰								
1, 2	1.63(2)	4.16(3)	-1.56(1)	-1.33(9)	-0.2(1)	-9.9(2)	-5.1(3)	-1.67(3)
3	1.51(5)	0.954(6)	-0.67(1)	-1.4(3)	4.2(2)	1.3(4)	-7.0(2)	-0.47(6)
4	1.72(3)	1.28(2)	-2.40(3)	3.8(1)	12.2(4)	0.00	0.00	0.00
5	1.55(6)	0.504(3)	-9.0(3)	1.9(1)	4.3(2)	0.00	0.00	0.00
6	1.44(4)	-2.35(5)	5.95(5)	3.3(1)	4.0(3)	0.00	0.00	0.00
7	1.03(5)	-2.9(3)	7.2(4)	0.3(1)	0.15(14)	0.00	0.00	0.00
$K_0 = 160.61(22) \text{ GPa}$, $K_0' = 4.09(2)$, $\theta_D = 940.38(40) \text{ K}$, $A^0(T_0) = -609.267(630) \text{ kJ mol}^{-1}$								
Debye: θ_D only volume dependent, third order Birch–Murnaghan eos								
	1.39(1)	1.38(5)	0.49(16)	0.00	0.00	0.00	0.00	0.00
$K_0 = 160.56(26) \text{ GPa}$, $K_0' = 4.04(3)$, $\theta_D = 763.84(90) \text{ K}$, $A^0(T_0) = -609.267(630) \text{ kJ mol}^{-1}$								
Debye: intrinsic anharmonic effect in θ_D , third order Birch–Murnaghan eos								
	1.47(1)	1.44(5)	-0.83(19)	0.00	2.82(5)	-3.44(3)	-4.37(28)	-0.65(1)
$K_0 = 160.64(24) \text{ GPa}$, $K_0' = 4.04(2)$, $\theta_D = 764.00(40) \text{ K}$, $A^0(T_0) = -609.267(630) \text{ kJ mol}^{-1}$								

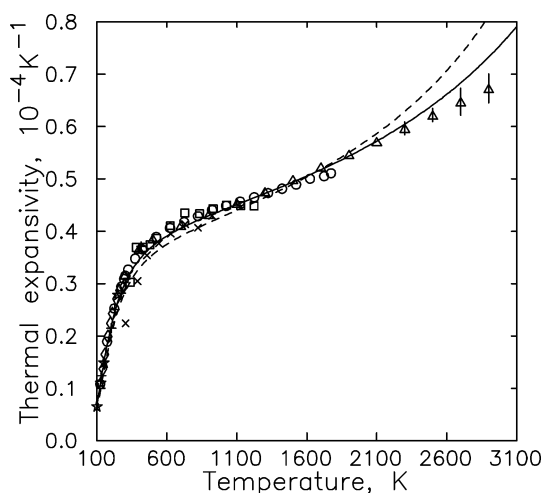


Fig. 3 Calculated thermal expansivity of MgO at 1 bar pressure together with experimental data of (□) Austin,¹⁵ (+) Durand,¹⁶ (×) Skinner,¹⁷ (◇) Ganesan,¹⁸ (○) Suzuki,¹⁹ and (△) Dubrovinsky and Saxena.²⁰ Data from White and Anderson,²¹ which are between those of Ganesan¹⁸ and Suzuki¹⁹ are omitted. The dashed curve represents a calculation with the Mie–Grüneisen–Debye (MGD) model where the cut-off frequency depends only on volume. The solid curves resulting from a MGD and a Kieffer model, which include intrinsic anharmonicity are indistinguishable.

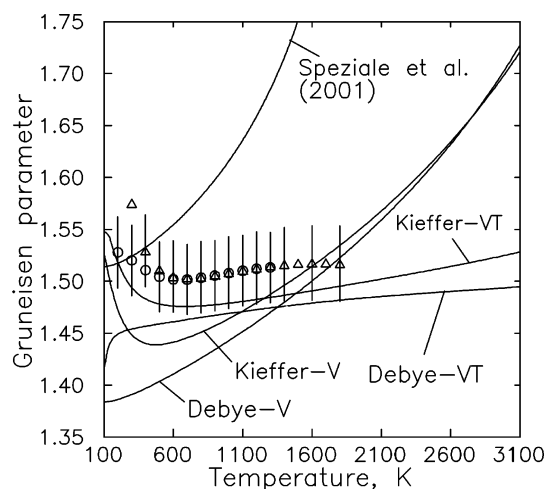


Fig. 4 Macroscopic Grüneisen parameter of MgO at 1 bar pressure. The data points were derived from experiments on adiabatic bulk modulus ((○) data from Sumino *et al.*,²³ (△) data from Isaak *et al.*²⁴), thermal expansivity, volume and heat capacity (C_p). The extension ‘-V’ denotes that the cut-off frequencies depend only on volume whereas the extension ‘-VT’ denotes the effect of intrinsic anharmonicity. The Debye temperature is 940 K.

behavior of the vibrational frequencies. Therefore special attention has been given to determine the minimum number of parameters, by means of statistical analysis. Table 2 indicates that we used 38 parameters in the Kieffer model whereas the MGD model requires only 10 parameters.

5.2 Volume and temperature dependence of cut-off frequencies

Fig. 4 indicates that in the MGD and Kieffer formalisms, the assumption of the quasi-harmonic approximation is not sufficient to describe experimental data at 1 bar pressure within experimental accuracy. A key to remedy the mismatch of the calculated and the experimental Grüneisen parameter is given by eqns. (15) and (16), which relate the acoustic sound velocities to the cut-off frequencies of the acoustic vibrational motions. Eqn. (15) puts forward that a cut-off frequency depending only on volume results in a behavior of the longitudinal sound velocity without an abrupt change in its volume derivative. To investigate this in more detail, we have plotted in Fig. 5 the longitudinal sound velocity as a function of volume derived from experimental measurements. The break in the slope of the longitudinal sound velocity indicates that the cut-off frequency depends not only on volume, within the accuracy of the measurements. The same conclusion applies to the transverse sound velocity provided that eqns. (15) and (16) are valid. However, when the transverse sound velocity is calculated using eqn. (17), the break in its slope is a result of the discontinuous behavior of the volume derivative of the bulk sound velocity. Although this discontinuity exists, the change in the volume derivative apparently does not adequately represent the data if it is assumed that the frequency depends on volume only. To proceed further, we used as working hypothesis that the cut-off frequencies change with temperature at constant volume. This implies a study on the possible effect of intrinsic anharmonicity. To obtain a description within the accuracy of the experiments applying a Kieffer model, the statistical evaluation of data revealed that intrinsic anharmonicity is not only present in acoustic but also in optic vibrations. Here we arrived at the unfortunate situation that no published experimental data are available on optic vibrational frequencies at temperatures higher than 300 K to further

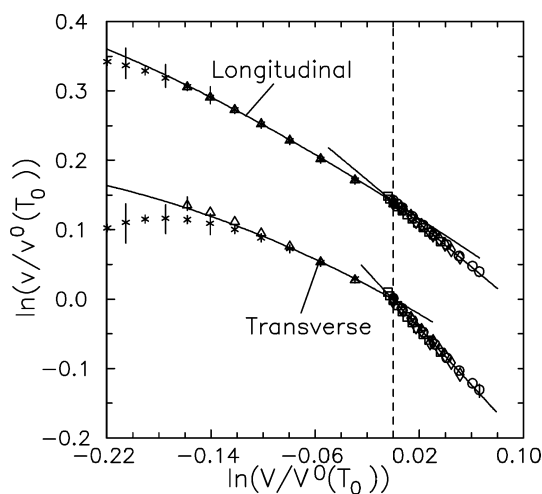


Fig. 5 The plot of the logarithm of longitudinal and transverse sound velocities against the logarithm of volume reveals a break in the slopes. $V^0(T_0)$ and $v^0(T_0)$ are the volume and sound velocities at room conditions. Measurements at 1 bar pressure, $V/V^0(T_0) > 1$, are from (\square) Sumino *et al.*,²³ (\circ) Isaak *et al.*,²⁴ and (\diamond) Sinogeikin *et al.*,²⁶ Measurements at 300 K, $V/V^0(T_0) < 1$, are from (\triangle) Chopelas¹² and ($*$) Zha *et al.*,²⁷ Error bars are equal to the symbol size unless they are plotted. The vertical dashed line indicates room conditions where $V = V^0(T_0) = 11.248 \text{ cm}^3$. The solid curves have been calculated with the values in Table 3 and eqns. (14), (15) and (16).

constrain our calculations. For the MGD model we proceeded in an analogous way by considering intrinsic anharmonicity in the Debye cut-off frequency. Fig. 4 shows the enormous increase in accuracy of the representation of the Grüneisen parameter when our hypothesis is put to work. It also demonstrates that Kieffer's model represents the Grüneisen parameter better than a MGD model. This is mainly due to a better representation of the heat capacity (C_p), see Fig. 6. Fig. 6 and Table 3 show that above room temperature the experimental heat capacity data of Krupka *et al.*,³² and those of Bosenick *et al.*,³³ are represented within the stated experimental accuracy of 1%. Only one experimental point in the data set of Bosenick *et al.*,³³ shows a difference with the calculated result of 5%. The experimental data of Richet and Fiquet³⁰ deviate by about 1.5% from those of Bosenick *et al.*,³³ in the temperature range between 816 and 972 K. Therefore our calculations differ by more than 1% from the experimental results of Richet and Fiquet.³⁰ A Kieffer model represents the experimental data of Barron *et al.*,³¹ better than a MGD model, but both models do not describe the data within the experimental accuracy of 0.2%. Additional calculations, in which the representation of these low temperature capacity data is forced to be accurate within 0.2%, showed that thermal expansivity, bulk modulus and sound velocity data could not be described within experimental accuracy. We consider the difference between calculated and experimental heat capacity of Barron *et al.*,³¹ a remaining artifact of our descriptions of MgO with a Kieffer and MGD model. In spite of this difference, the calculated standard entropy at 298.15 K, 26.917 J K⁻¹ mol⁻¹ for the MGD model and 26.922 J K⁻¹ mol⁻¹ for the Kieffer model respectively, is in good agreement with the experimental value of $26.924 \pm 0.08 \text{ J K}^{-1} \text{ mol}^{-1}$ (see JANAF thermochemical Tables, Chase *et al.*,²⁵).

We conclude that the VDOS only slightly influences the accuracy of the description of thermodynamic data. The calculations were performed using the values in Table 2 for the constants in eqn. (14) and equation of state parameters. The characteristic frequencies of the vibrational modes and their weight fractions are given in Table 1.

The incorporation of intrinsic anharmonicity results in a deviation of the heat capacity at constant volume, C_V , from

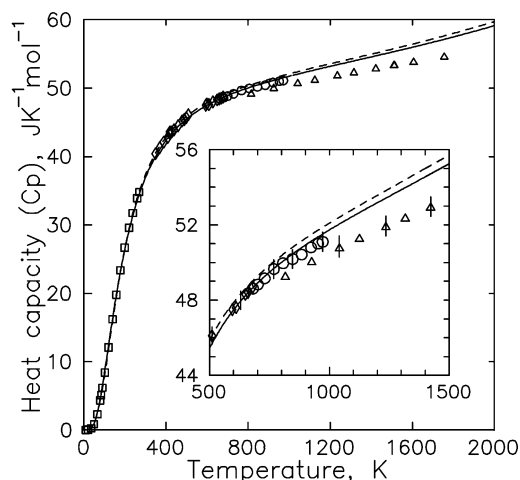


Fig. 6 Calculated heat capacity (C_p) of MgO at 1 bar pressure compared with experimental data from: (\square) Barron *et al.*,³¹ (\diamond) Krupka *et al.*,³² (\triangle) Richet and Fiquet³⁰ and (\circ) Bosenick *et al.*,³³ The dashed curve represents the calculation with a MGD model and the solid curve has been calculated with a Kieffer model. Both models include intrinsic anharmonicity. The inset gives a comparison between calculated and experimental C_p data in the temperature range between 500 and 1500 K.

Table 3 Representation of experimental thermodynamic data by a Kieffer and a Mie–Grüneisen–Debye model. The input properties used in the calculations are given in Tables 1 and 2

Property	Maximum absolute deviation (%)	Average absolute deviation (%)	Temperature range/K	Pressure range/GPa	Reference
Adiabatic bulk modulus	1.57, ^a 1.39 ^b	0.73, ^a 0.67 ^b	300–1800	0.0	Isaak <i>et al.</i> ²⁴
	0.62, ^a 0.56 ^b	0.16, ^a 0.15 ^b	100–1300	0.0	Sumino <i>et al.</i> ²³
	0.94, ^a 0.93 ^b	0.33, ^a 0.30 ^b	295–1510	0.0	Sinogeikin <i>et al.</i> ²⁶
	2.77, ^a 2.81 ^b	0.91, ^a 0.93 ^b	300	0.0–30	Duffy and Ahrens ²⁸
	2.73, ^a 2.78 ^b	1.07, ^a 1.09 ^b	300	0.0–30	Chopelas ¹²
	1.14, ^a 1.09 ^b	0.57, ^a 0.57 ^b	300	0.0–55	Zha <i>et al.</i> ²⁷
	1.53, ^a 1.56 ^b	0.62, ^a 0.63 ^b	300	0.0–18.6	Sinogeikin and Bass ²⁹
	Heat capacity (C_p)	4.48, ^a 5.44 ^b	3.00, ^a 3.90 ^b	816–1756	0.0
9.00, ^a 69.00 ^b		4.52, ^a 12.50 ^b	0.0–140	0.0	Barron <i>et al.</i> ³¹
0.74, ^a 2.15 ^b		0.59, ^a 0.75 ^b	140–269	0.0	Barron <i>et al.</i> ³¹
0.96, ^a 0.88 ^b		0.42, ^a 0.57 ^b	350–680	0.0	Krupka <i>et al.</i> ³²
5.09, ^a 5.84 ^b		0.49, ^a 0.90 ^b	332–972	0.0	Bosenick <i>et al.</i> ³³
Volume	1.36, ^a 1.38 ^b	0.22, ^a 0.22 ^b	298–3000	0.0	Dubrovinsky and Saxena ²⁰
	0.46, ^a 0.47 ^b	0.15, ^a 0.15 ^b	298–2973	0.0	Fiquet <i>et al.</i> ²²
	1.39, ^a 1.41 ^b	0.29, ^a 0.30 ^b	300–2475	0.0–53.0	DeWaele <i>et al.</i> ³⁴
	0.29, ^a 0.29 ^b	0.11, ^a 0.11 ^b	300	0.0–52.2	Speziale <i>et al.</i> ³⁵
	3.35, ^a 3.35 ^b	1.78, ^a 1.78 ^b	300	43.7–94.1	Mao and Bell ³⁶
	4.62, ^a 4.62 ^b	4.05, ^a 4.05 ^b	300	159–198	Vassilou and Ahrens ³⁷
	1.97, ^a 1.96 ^b	1.16, ^a 1.16 ^b	300	19–121	Carter <i>et al.</i> ³⁸
	0.99, ^a 0.98 ^b	0.59, ^a 0.58 ^b	300	0.0–35	Perez-Albuera and Drickamer ³⁹
	1.91, ^a 1.91 ^b	1.39, ^a 1.38 ^b	300	14–132	Duffy and Ahrens ⁴⁰
	0.28, ^a 0.28 ^b	0.13, ^a 0.13 ^b	300–1100	0.0–25.5	Fei <i>et al.</i> ⁴¹
	0.06, ^a 0.06 ^b	0.03, ^a 0.04 ^b	300	0.0–55	Zha <i>et al.</i> ²⁷
	0.46, ^a 0.51 ^b	0.13, ^a 0.14 ^b	300–3000	0.0–100	Matsui <i>et al.</i> ⁴²
	2.22, ^a 2.30 ^b	1.99, ^a 2.06 ^b	3071–3663	174–203	Svendsen and Ahrens ⁴³
	3.10, ^a 3.10 ^b	1.50, ^a 1.50 ^b	300	0.0–227.0	Duffy <i>et al.</i> ⁴⁴
	Thermal expansion	4.17, ^a 12.12 ^b	2.07, ^a 2.91 ^b	123–1773	0.0
9.57, ^a 8.44 ^b		2.82, ^a 2.72 ^b	300–3000	0.0	Dubrovinski and Saxena ²⁰
8.54, ^a 9.25 ^b		3.19, ^a 3.31 ^b	335–1221	0.0	Austin ¹⁵
5.73, ^a 7.44 ^b		2.81, ^a 5.33 ^b	146–288	0.0	Ganesan ¹⁸
5.64, ^a 14.21 ^b		2.74, ^a 4.65 ^b	129–416	0.0	Durand ¹⁶
35.32, ^a 33.52 ^b		7.00, ^a 6.61 ^b	304–923	0.0	Skinner ¹⁷
34.48, ^a 39.98 ^b		30.53, ^a 35.82 ^b	2000	169–196	Duffy and Ahrens ⁴⁰
14.33, ^a 14.51 ^b		9.40, ^a 9.73 ^b	2000	0–100	Isaak <i>et al.</i> ⁴⁵
3.74, ^a 1.89 ^b		1.80, ^a 0.93 ^b	2000	0–135	Wang and Reeber ⁴⁶
8.53, ^a 10.51 ^b		4.39, ^a 6.29 ^b	2000	20–120	Chopelas and Boehler ⁴⁷
Bulk sound velocity	1.78, ^a 1.80 ^b	0.92, ^a 0.93 ^b	300	0.0–35	Chopelas ¹²
	1.72, ^a 1.74 ^b	1.20, ^a 1.20 ^b	300	0.0–30	Duffy and Ahrens ²⁸
	0.91, ^a 0.91 ^b	0.39, ^a 0.40 ^b	300	0.0–55	Zha <i>et al.</i> ²⁷
	0.89, ^a 0.80 ^b	0.40, ^a 0.38 ^b	300–1300	0.0	Isaak <i>et al.</i> ²⁴
	0.23, ^a 0.26 ^b	0.06, ^a 0.08 ^b	100–1300	0.0	Sumino <i>et al.</i> ²³
	0.45, ^a 0.44 ^b	0.17, ^a 0.15 ^b	295–1510	0.0	Sinogeikin <i>et al.</i> ²⁶

^a Kieffer model. ^b Mie–Grüneisen–Debye model.

the Dulong–Petit relation. This deviation is 1.5% at 2000 K and 3.5% at 2500 K.

5.3 The role of the equation of state

Table 3 shows that both a Mie–Grüneisen–Debye (MGD) as well as a Kieffer model of the vibrational density of states accurately represent thermodynamic data, provided that intrinsic mode anharmonicity is included in the description. Fig. 7 visualizes the deviations between calculated and experimentally established volume data given in Table 3. All deviations are commensurate with experimental errors except for the shockwave data measured by Svendsen and Ahrens.⁴³ Representing their data within the stated experimental accuracy of 1% requires a value of about 4.5 for the pressure derivative of the isothermal bulk modulus (K'_0). This value is too high compared to values established from diamond anvil experi-

ments, 3.94 ± 0.2 by DeWaele *et al.*,³⁴ 3.99 ± 0.01 by Speziale *et al.*³⁵ and 4.03 ± 0.03 by Zha *et al.*²⁷ Speziale *et al.*³⁵ found a satisfactory description of their own volume data at 300 K, those of DeWaele *et al.*³⁴ and the shockwave data of Svendsen and Ahrens⁴³ by using a Mie–Grüneisen–Debye model. However, Fig. 4 indicates that data at 1 bar pressure are not reproduced well. This compelled us to investigate the role of the equation of state, given by the term $P^{\text{eos}}(T_0, V)$ in eqn. (7). Instead of a third order Birch–Murnaghan equation of state we used the equation of state given by Jacobs and Oonk,¹⁰ which is based on an empirical relation between volume and bulk modulus. We used this equation of state in combination with Kieffer's model. Not surprisingly the results of the calculations given in Table 2 indicate that K'_0 increases slightly relative to the experimental values between 3.94 and 4.03, because these values were established with a third order Birch–Murnaghan equation of state. It appears that the use of the

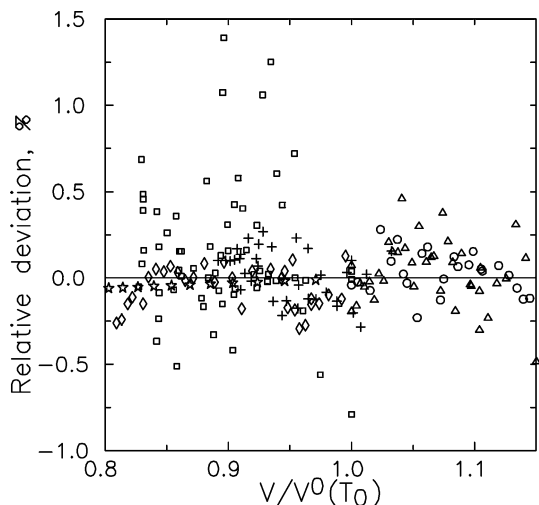


Fig. 7 Relative deviations of calculated and experimental volumes compared with experimental data from: (O) Dubrovinsky and Saxena,²⁰ (+) Fei *et al.*,⁴¹ (Δ) Fiquet *et al.*,²² (\square) DeWaele *et al.*,³⁴ (*) Zha *et al.*,²⁷ and (\diamond) Speziale *et al.*³⁵ There is no significant difference in the representation of volume data between a Kieffer model and MGD model.

equation of state given by Jacobs and Oonk¹⁰ neither has significant influence on the representation of shockwave data of Svendsen and Ahrens⁴³ nor on the representation of all other thermodynamic data in Table 3. The same conclusion applies to the description of the sound wave velocities presented in Table 4. In addition, on applying the third order Birch–Murnaghan equation of state and the equation of state given by Jacobs and Oonk,¹⁰ we arrived at the same VDOS parameters given in Table 1. This indicates that the use of a different equation of state does not affect the VDOS significantly.

5.4 Sound wave velocities

Because adiabatic bulk modulus and volume are represented well by the MGD and Kieffer model, the bulk sound velocity,

plotted in Fig. 8 and 9, is represented within experimental accuracy for both the isothermal and the isobaric direction.

In our optimization of experimental thermodynamic data with the MGD model we have fitted the Debye temperature. The calculated value of about 764 K deviates considerably from the experimentally established value of 940 K by White and Anderson,²¹ 941 ± 10 K by Sumino *et al.*²³ and 945 ± 2 by Isaak *et al.*²⁴ As a result the mean sound velocity, v_m , deviates from the experimental value. This can be made visible through Debye's classical relation (Debye⁴⁸):

$$v_m = \frac{k\theta_D}{h} \left(\frac{3nN_A}{4\pi ZV} \right)^{-1/3} = \left[\frac{1}{3} \left(\frac{2}{v_T^3} + \frac{1}{v_L^3} \right) \right]^{-1/3}. \quad (18)$$

The simple shape of the VDOS depicted in Fig. 2 resulting from the MGD model is apparently not sufficient to comprise a reliable description of thermodynamic data as well as a mean sound velocity given by acoustic experiments. The situation is different in Kieffer's model in which Kieffer^{7,8} has calculated values for u_1 , u_2 and u_3 appearing in eqns. (15) and (16) leading to a mean sound velocity consistent with the experimental value of White and Anderson.²¹ Eqn. (18) puts forward that the mean sound velocity is correctly described provided that the longitudinal and transverse sound velocities have been accurately determined. The longitudinal sound velocity ($v_L = u_3$) and the transverse sound velocity, resulting from eqn. (15) and (16) respectively, are plotted in Fig. 8 and 9. These velocities are in excellent agreement with experiments. The same holds true when the transverse sound velocity is calculated from eqn. (17). The deviation between calculated transverse sound velocities by eqn. (16) and (17) is less than 1.5% in the experimental data range. The longitudinal and transverse sound velocities increase isothermally with pressure and decrease isobarically with temperature in the temperature range between 100 and 4000 K and pressure range between 1 bar and 300 GPa.

6 Conclusions

Within the framework of a Mie–Grüneisen–Debye or Kieffer formalism, the quasi-harmonic approximation appears to

Table 4 The representation of sound velocity and shear modulus data by a Kieffer model. For the transverse sound velocity we used eqn. (17) and eqn. (16). Calculations with eqn. (16) are italicised. The input properties used in the calculation are given in Tables 1 and 2

Property	Maximum absolute deviation (%)	Average absolute deviation (%)	Temperature range/K	Pressure range/GPa	Reference
Longitudinal sound velocity	4.92	1.67	300	0.0–30	Duffy and Ahrens ²⁸
	0.19	0.1	300	0.0–40	Chopelas ¹²
	1.78	0.44	300	0.0–55	Zha <i>et al.</i> ²⁷
	0.24	0.1	300–1800	0.0	Isaak <i>et al.</i> ²⁴
	0.31	0.24	100–1300	0.0	Sumino <i>et al.</i> ²³
	0.27	0.12	295–1510	0.0	Sinogeikin <i>et al.</i> ²⁶
Transverse sound velocity	1.81, <i>0.57</i>	1.06, <i>0.33</i>	300	0.0–40	Chopelas ¹²
	4.11, <i>5.04</i>	1.05, <i>1.81</i>	300	0.0–55	Zha <i>et al.</i> ²⁷
	1.25, <i>0.54</i>	0.32, <i>0.30</i>	300–1800	0.0	Isaak <i>et al.</i> ²⁴
	0.64, <i>0.43</i>	0.43, <i>0.39</i>	100–1300	0.0	Sumino <i>et al.</i> ²³
	0.71, <i>0.95</i>	0.21, <i>0.34</i>	295–1510	0.0	Sinogeikin <i>et al.</i> ²⁶
Shear modulus	3.03, 5.88	0.91, 2.97	300	0.0–30	Duffy and Ahrens ²⁸
	3.23, 0.92	1.84, 0.53	300	0.0–35	Chopelas ¹²
	7.37, 9.30	2.42, 3.49	300	0–55	Zha <i>et al.</i> ²⁷
	0.72, 3.32	0.43, 2.25	300	0.0–18.6	Sinogeikin and Bass ²⁹
	2.41, 1.13	0.54, 0.65	300–1800	0.0	Isaak <i>et al.</i> ²⁴
	1.19, 1.26	0.77, 0.84	100–1300	0.0	Sumino <i>et al.</i> ²³
	1.78, 2.02	0.44, 0.70	295–1510	0.0	Sinogeikin <i>et al.</i> ²⁶
Mode frequencies	0.509	0.19	300	0.0–35	Chopelas ¹²

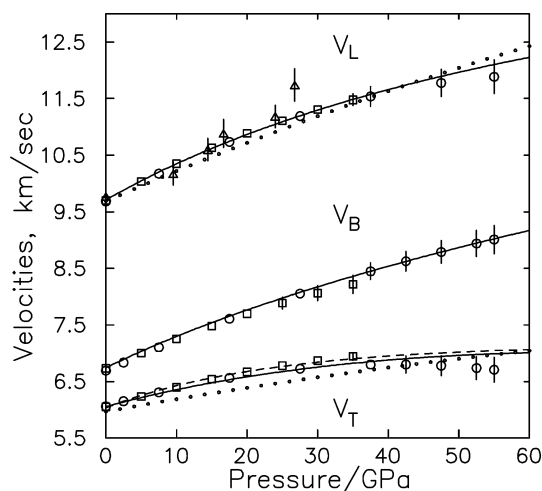


Fig. 8 Calculated longitudinal (V_L), bulk (V_B) and transverse (V_T) sound velocities compared with the experiments of (\square) Chopelas,¹² (\circ) Zha *et al.*²⁷ and (\triangle) Duffy and Ahrens.²⁸ Error bars are equal to the symbol size unless they are plotted. The dotted curves corresponding to theoretical calculations of Karki *et al.*⁴⁹ are given for comparison. The solid curve for the transverse sound velocity has been calculated with the quadratic expression, eqn. (17) and the dashed curve with the cubic expression, eqn. (16). The deviation between these curves is less than 1.5%.

be insufficient to represent thermodynamic data and sound velocities within experimental accuracy.

When the effect of intrinsic anharmonicity is introduced, the simple expression for the vibrational density of states within the framework of a Mie–Grüneisen–Debye formalism suffices to represent thermodynamic data within experimental accuracy. However, the acoustic mean sound wave velocities are not represented accurately.

Within the framework of a Kieffer formalism, a simplified vibrational density of states is sufficient to represent thermodynamic data and sound wave velocity data provided that the effect of intrinsic anharmonicity is included in acoustic and optic vibrational modes.

Both formalisms are not able to represent the high-temperature, high-pressure shockwave data of Svendsen and Ahrens.⁴³

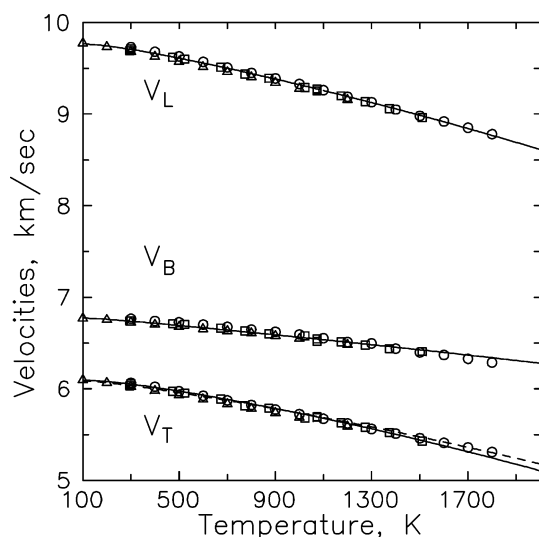


Fig. 9 Calculated longitudinal (V_L), bulk (V_B) and transverse (V_T) sound velocities compared with the experiments of (\triangle) Sumino *et al.*,²³ (\circ) Isaak *et al.*,²⁴ and (\square) Sinogeikin *et al.*²⁶ The solid curve for the transverse sound velocity has been calculated with the quadratic expression, eqn. (17) and the dashed curve with the cubic expression, eqn. (16). The deviation between these curves is less than 0.4%.

The application of the equation of state given by Jacobs and Oonk¹⁰ does not lead to a significant improvement in the representation of thermodynamic data and sound wave velocity data compared to the application of a third order Birch–Murnaghan equation of state.

In our descriptions using a Mie–Grüneisen–Debye or a Kieffer formalism, no anomalies are present in thermodynamic properties, shear modulus and sound wave velocities in the temperature range between 100 and 4000 K and the pressure range between 1 bar and 300 GPa.

Acknowledgements

This work was supported by the Netherlands Research Centre for Integrated Solid Earth Science. We express our gratitude to two anonymous reviewers for their helpful comments.

References

- 1 Y. Fei, H. Mao and B. O. Mysen, *J. Geophys. Res.*, 1991, **96**, 2157–2169.
- 2 S. K. Saxena, *Geochim. Cosmochim. Acta*, 1996, **60**, 2379–2395.
- 3 M. Gottschalk, *Eur. J. Mineral.*, 1997, **9**, 175–223.
- 4 N. D. Chatterjee, R. Kruger, G. Haller and W. Olbricht, *Contrib. Miner. Petrol.*, 1998, **133**, 149–168.
- 5 O. Fabricnaya, *Calphad*, 1998, **22**, 85–125.
- 6 T. J. B. Holland and R. Powell, *J. Metamorph. Geol.*, 1998, **16**, 309–343.
- 7 S. W. Kieffer, *Rev. Geophys. Space Phys.*, 1979, **17**, 1–19.
- 8 S. W. Kieffer, *Rev. Geophys. Space Phys.*, 1979, **17**, 35–59.
- 9 I. Jackson and S. M. Rigden, *Phys. Earth Planet. Int.*, 1996, **96**, 85–112.
- 10 M. H. G. Jacobs and H. A. J. Oonk, *Phys. Chem. Chem. Phys.*, 2000, **2**, 2641–2646.
- 11 E. Grüneisen, *Handb. Phys.*, 1926, **10**, 1–59.
- 12 A. Chopelas, *Phys. Chem. Miner.*, 1996, **23**, 25–37.
- 13 P. Gillet, I. Daniel, F. Guyot, J. Matas and J-C. Chervin, *Phys. Earth Planet. Int.*, 2000, **117**, 361–384.
- 14 M. J. L. Sangster, G. Peckham and D. H. Saunderson, *J. Phys. Chem.*, 1970, **3**, 1026–1036.
- 15 J. B. Austin, *J. Am. Ceram. Soc.*, 1931, **14**, 795–810.
- 16 M. A. Durand, *Physics*, 1936, **7**, 297–298.
- 17 B. J. Skinner, *Am. Mineral.*, 1957, **42**, 39–55.
- 18 S. Ganesan, *Philos. Mag.*, 1962, **7**, 197–205.
- 19 I. Suzuki, *J. Phys. Earth*, 1975, **23**, 145–159.
- 20 L. S. Dubrovinsky and S. K. Saxena, *Phys. Chem. Miner.*, 1997, **24**, 547–550.
- 21 G. K. White and O. L. Anderson, *J. Appl. Phys.*, 1966, **37**, 430–432.
- 22 G. Fiquet, P. Richet and G. Montagnac, *Phys. Chem. Miner.*, 1999, **27**, 103–111.
- 23 Y. Sumino, O. L. Anderson and I. Suzuki, *Phys. Chem. Miner.*, 1983, **9**, 38–47.
- 24 D. G. Isaak, O. L. Anderson and T. Goto, *Phys. Chem. Miner.*, 1989, **16**, 704–713.
- 25 M. W. Chase Jr, C. A. Davies, J. R. Downey Jr, D. J. Frurip, R. A. McDonald and A. N. Syverud, *J. Phys. Chem. Ref. Data*, 1985, **14**(Suppl. 1), 1469–1472.
- 26 S. V. Sinogeikin, J. M. Jackson, B. O'Neill, J. W. Palko and J. D. Bass, *Rev. Sci. Instrum.*, 2000, **71**, 201–206.
- 27 C-S. Zha, H-K. Mao and R. J. Hemley, *Proc. Natl. Acad. Sci. USA*, 2000, **97**, 13494–13499.
- 28 T. S. Duffy and T. J. Ahrens, *J. Geophys. Res.*, 1995, **100**, 529–542.
- 29 S. V. Sinogeikin and J. D. Bass, *Phys. Rev. B.*, 1999, **59**, 14141–14144.
- 30 P. Richet and G. Fiquet, *J. Geophys. Res.*, 1991, **96**, 445–456.
- 31 T. H. K. Barron, W. T. Berg and J. A. Morrison, *Proc. R. Soc. London A*, 1959, **250**, 70–83.
- 32 K. M. Krupka, R. A. Robie and B. S. Hemingway, *Am. Mineral.*, 1979, **64**, 86–101.
- 33 A. Bosenick, C. A. Geiger and L. Cemič, *Geochim. Cosmochim. Acta*, 1996, **60**, 3215–3227.
- 34 A. DeWaele, G. Fiquet, D. Andrault and D. Häusermann, *J. Geophys. Res.*, 2000, **105**, 2869–2877.

- 35 S. Speziale, C-S Zha, T. S. Duffy, R. J. Hemley and H-K Mao, *J. Geophys. Res.*, 2001, **106**, 515–528.
- 36 H. K. Mao and P. M. Bell, *J. Geophys. Res.*, 1979, **84**, 4533–4536.
- 37 M. S. Vassilou and T. J. Ahrens, *Geophys. Res. Lett.*, 1981, **8**, 729–732.
- 38 W. T. Carter, S. P. Marsh, J. N. Fitz and R. G. McQueen, in *Accurate Characterization of the High Pressure environment*, ed. E. C. Lloyd, NBS special pub. 326, Washington D.C., 1971, p. 147.
- 39 E. A. Perez-Albuerne and H. G. Drickamer, *J. Chem. Phys.*, 1965, **43**, 1381–1387.
- 40 T. S. Duffy, T. J. Ahrens, in, J. Z. Hu, H. K. Mao, J. Shu and R. J. Hemley, *High-Pressure Science and Technology*, ed. S. C. Schmidt, J. W. Shaner, G. A. Samara and M. Ross, AIP, New York, 1994, p. 1107.
- 41 Y. Fei, *Am. Mineral.*, 1999, **84**, 272–276.
- 42 M. Matsui, S. C. Parker and M. Leslie, *Am. Mineral.*, 2000, **85**, 312–316.
- 43 B. Svendsen and T. J. Ahrens, *Geophys. J. R. Astron. Soc.*, 1987, **91**, 667–691.
- 44 T. S. Duffy, R. J. Hemley and H. K. Mao, *Phys. Rev. Lett.*, 1995, **74**, 1371–1374.
- 45 D. G. Isaak, R. E. Cohen and M. J. Mehl, *J. Geophys. Res.*, 1990, **95**, 7067.
- 46 K. Wang and R. R. Reeber, *Geophys. Res. Lett.*, 1995, **22**, 1297–1300.
- 47 A. Chopelas and R. Boehler, *Geophys. Res. Lett.*, 1992, **19**, 1983–1986.
- 48 P. Debye, *Ann. Der Phys.*, 1912, **39**, 789–839.
- 49 B. B. Karki, L. Stixrude, S. J. Clark, M. C. Warren, G. J. Auckland and J. Crain, *Am. Mineral.*, 1997, **82**, 51–60.